

# Searching for the LFV $\gamma\gamma e\mu$ interaction at $e^-e^+$ colliders

M. A. Arroyo-Ureña,<sup>1,2,\*</sup> R. Gaitán,<sup>3,†</sup> Marcela Marín,<sup>3,‡</sup>  
Humberto Salazar,<sup>1,2,§</sup> and M. G. Villanueva-Utrilla<sup>1,2,¶</sup>

<sup>1</sup>*Facultad de Ciencias Físico-Matemáticas and*

<sup>2</sup>*Centro Interdisciplinario de Investigación y Enseñanza de la Ciencia (CIEC),  
Benemérita Universidad Autónoma de Puebla, C.P. 72570, Puebla, México,*

<sup>3</sup>*Departamento de Física, FES-Cuautitlán,  
UNAM, C.P. 54770, Estado de México, México,*

## Abstract

We study the possibility of detecting the Lepton Flavor Violating (LFV) process  $e^-e^+ \rightarrow e^-e^+e\mu$  ( $e = e^-, e^+$ ;  $\mu = \mu^-, \mu^+$ ) at the forthcoming  $e^-e^+$  colliders Compact Linear Collider (CLIC) and the International Linear Collider (ILC). Our predictions are based on an effective operator framework that induces the LFV interaction  $\gamma\gamma e\mu$ . According to three benchmark points that are consistent with theoretical and current experimental constraints, we find that all of them are experimentally feasible, predicting *signal significances*  $\mathcal{S} \geq 5\sigma$  at both colliders for relatively low integrated luminosities and center-of-mass energies between 500 – 1000 GeV.

---

\* [marco.arroyo@fcfm.buap.mx](mailto:marco.arroyo@fcfm.buap.mx)

† [rgaitan@unam.mx](mailto:rgaitan@unam.mx)

‡ [marcemarino8a@cuautitlan.unam.mx](mailto:marcemarino8a@cuautitlan.unam.mx)

§ [hsalazar@fcfm.buap.mx](mailto:hsalazar@fcfm.buap.mx)

¶ [maria.villanueva@alumno.buap.mx](mailto:maria.villanueva@alumno.buap.mx)

## I. INTRODUCTION

In the Standard Model (SM), lepton flavor is strictly conserved in its original formulation with massless neutrinos. However, the observation of neutrino oscillations has firmly established that these particles possess nonzero masses [1–3], implying lepton flavor violation in the neutral sector. Although the SM —augmented by nonzero neutrino masses— predicts charged LFV (cLFV) processes to occur at extremely suppressed rates due to the GIM mechanism [4], any definitive experimental observation of cLFV would provide incontrovertible evidence for physics beyond the SM. Over the past eight decades, extensive experimental efforts have been dedicated to searching for cLFV processes [5–7] without a conclusive response. In this work, we explore the  $\gamma\gamma e\mu$  interaction, arising within a low-energy Effective Field Theory (EFT) framework, and assess its prospects for experimental investigation at the CLIC [8] and ILC [9].

Photon–photon interactions provide a remarkably clean probe of electromagnetic phenomena, as they are precisely described by Quantum Electrodynamics (QED) and effectively modeled through the equivalent photon approximation (EPA) [10–12]. In electron–positron colliders, the  $e^+$  and  $e^-$  beams act as sources of quasi–real photons, enabling precise measurements of processes such as Breit–Wheeler  $e^+e^-$  pair production [13–15] and exclusive dimuon production [16, 17]. These well–established measurements provide stringent tests of QED and serve as essential benchmarks for the search for rare phenomena, including cLFV via processes like  $\gamma\gamma \rightarrow e\mu$ . Moreover, the extraordinarily clean environment of electron–positron colliders —characterized by high luminosity and low background— enhances the potential to probe the  $\gamma\gamma e\mu$  interaction. In this context, CLIC and ILC offer complementary regimes: both colliders plan unprecedented high centre-of-mass energies, up to 3 TeV and 1 TeV<sup>1</sup>, respectively. Their high luminosities also may considerably increase the number of events produced, up to 2.5 ab<sup>−1</sup> at  $\sqrt{s} = 1.5$  TeV for CLIC and 4 ab<sup>−1</sup> at  $\sqrt{s} = 0.5$  TeV for ILC. Other possible scenarios would be the Circular Electron–Positron Collider (CEPC) [18] and the Future Circular Collider (FCC) [19]. However, as will be seen later, the energy achieved at these colliders will not be sufficient to produce the number of signal events necessary to have evidence of the  $\gamma\gamma e\mu$  interaction.

The theoretical framework adopted in this work can induce the radiative decays  $\ell_i \rightarrow \ell_j \gamma(\gamma)$ , cLFV conversions in nuclei, three-body decays  $\ell_i \rightarrow \ell_j \bar{\ell}_k \ell_k$ , and semileptonic tau decays  $\tau \rightarrow \ell PP$ , where  $PP$  denotes a pair of light pseudoscalar mesons. A comparative analysis with current experimental bounds, as presented in Ref. [20], reveals that the most stringent constraints on the diphoton operators arise from the loop-induced radiative decays  $\ell_i \rightarrow \ell_j \gamma$  [21–23]. However, despite the suppression of the parameters in the theory, we identify a region of the parameter space in which the couplings that directly affect the proposed signal are favorable to motivate searches for the experimental cLFV process via photon–photon scattering at the colliders aforementioned.

This letter is structured as follows. In Sec. II section\*.4, we present the theoretical framework in which our predictions are based. Experimental constraints on the model parameter space are also

---

<sup>1</sup> According to reports, there will be a possible energy increase of up to 1 TeV [9]. In this work, we also explore such a scenario.

included. Section III section\*.8 focuses on taking advantage of the insights gained from previous section, performing a computational analysis of the proposed signal and its SM background processes. Finally, the conclusions are presented in Sec. IV section\*.16.

## II. THEORETICAL FRAMEWORK

The local charged lepton flavor violating interaction  $\gamma\gamma\bar{\ell}_i\ell_j$  is described by the effective Lagrangian [24, 25]:

$$\begin{aligned}\mathcal{L}_{\text{eff}} = & \left( G_{SR}^{ij} \bar{\ell}_{L_i} \ell_{R_j} + G_{SL}^{ij} \bar{\ell}_{R_i} \ell_{L_j} \right) F_{\mu\nu} F^{\mu\nu} \\ & + \left( \tilde{G}_{SR}^{ij} \bar{\ell}_{L_i} \ell_{R_j} + \tilde{G}_{SL}^{ij} \bar{\ell}_{R_i} \ell_{L_j} \right) \tilde{F}_{\mu\nu} F^{\mu\nu} + \text{H.c.},\end{aligned}\quad (2.1)$$

where  $\ell_i, \ell_j = e, \mu, \tau$  denote the lepton flavors, and  $F_{\mu\nu}$  and  $\tilde{F}_{\mu\nu} = \frac{1}{2}\epsilon_{\mu\nu\sigma\lambda}F^{\sigma\lambda}$  are the electromagnetic field strength tensor and its dual, respectively. The operators involve left- and right-handed chiral components of the leptons, with  $G_{SR}^{ij}$ ,  $G_{SL}^{ij}$ ,  $\tilde{G}_{SR}^{ij}$ , and  $\tilde{G}_{SL}^{ij}$  parameterizing the interaction strengths. These effective couplings are dimensionful quantities, scaling as  $1/\Lambda^3$ , where  $\Lambda$  is the cutoff energy scale of the EFT. This scaling behavior is consistent with the suppression expected for dimension-7 operators in an EFT extension of the SM, where LFV interactions are forbidden at tree level but can arise in new physics models. The dual field strength tensor  $\tilde{F}_{\mu\nu}$  introduces additional complexity to the operator structure, which remains underexplored in the literature, thereby offering the potential for new LFV channels in high-energy experiments.

### A. EFT parameter space

At the level of the effective Lagrangian, the decay  $\ell_i \rightarrow \ell_j \gamma$  is generated at the one-loop level [26]. For the purposes of numerical analysis, it suffices to focus on the leading logarithmic contributions to the decay rate, which can be expressed as:

$$\Gamma(\ell_i \rightarrow \ell_j \gamma) \sim \frac{\alpha |G_{ij}|^2}{256\pi^4} m_i^7 \log^2 \left( \frac{\Lambda^2}{m_i^2} \right), \quad (2.2)$$

where  $m_i$  is the mass of the decaying lepton, and the final-state lepton mass has been neglected for simplicity. The effective coupling  $|G_{ij}|$  encapsulates the relevant operator coefficients and it is defined as:

$$|G_{ij}|^2 = |G_{SL}^{ij}|^2 + |G_{SR}^{ij}|^2 + |\tilde{G}_{SL}^{ij}|^2 + |\tilde{G}_{SR}^{ij}|^2. \quad (2.3)$$

A key feature of this result is the apparent non-decoupling behavior, which manifests as a logarithmic enhancement of the decay rate. However, this embossing is naturally mitigated by the  $1/\Lambda^3$  suppression of the dimensionful couplings  $G_{ij}$ , consistent with the scaling behavior expected in an EFT framework. This interplay ensures the theoretical consistency of the EFT

description while providing a robust prediction for cLFV observables.

From the decay rate in Eq. (2.2equation.2.2) and the upper limits on  $\text{BR}(\ell_i \rightarrow \ell_j \gamma)$  [21–23], we derive stringent constraints on the effective couplings  $|G_{ij}|$ :

$$\begin{aligned} |G_{\mu e}| &\lesssim 1.2 \times 10^{-10} \left( 1 + 0.15 \ln \frac{\Lambda}{100 \text{ GeV}} \right)^{-1} \text{ GeV}^{-3}, \\ |G_{\tau e}| &\lesssim 8.4 \times 10^{-9} \left( 1 + 0.25 \ln \frac{\Lambda}{100 \text{ GeV}} \right)^{-1} \text{ GeV}^{-3}, \\ |G_{\tau \mu}| &\lesssim 9.5 \times 10^{-9} \left( 1 + 0.25 \ln \frac{\Lambda}{100 \text{ GeV}} \right)^{-1} \text{ GeV}^{-3}, \end{aligned} \quad (2.4)$$

where the bounds exhibit a mild logarithmic dependence on the cutoff scale  $\Lambda$ .

We now introduce nonchiral coefficients, which are more convenient for Monte Carlo simulations. The scalar and pseudoscalar coefficients are defined as:

$$\begin{aligned} G_S^{ij} &= \frac{G_{SR}^{ij} + G_{SL}^{ij}}{2}, & G_P^{ij} &= \frac{G_{SR}^{ij} - G_{SL}^{ij}}{2}, \\ \tilde{G}_S^{ij} &= \frac{\tilde{G}_{SR}^{ij} + \tilde{G}_{SL}^{ij}}{2}, & \tilde{G}_P^{ij} &= \frac{\tilde{G}_{SR}^{ij} - \tilde{G}_{SL}^{ij}}{2}, \end{aligned} \quad (2.5)$$

which leads us to derive the following constraint:

$$|G_{ij}|^2 = 2(|G_P^{ij}|^2 + |G_S^{ij}|^2 + |\tilde{G}_P^{ij}|^2 + |\tilde{G}_S^{ij}|^2) \quad (2.6)$$

From Eqs. (2.4equation.2.4) and (2.6equation.2.6), we obtain the parameter space in the  $|G_S^{e\mu}| - |G_P^{e\mu}|$  plane, which is presented in Fig. 1Parameter space in the  $|G_S^{e\mu}| - |G_P^{e\mu}|$  plane. The blue points are these allowed by constraints in Eqs. (2.4equation.2.4) and (2.6equation.2.6).figure.caption.6. Our approach to generating the parameter space involves scanning the set  $\{|G_S^{e\mu}|, |G_P^{e\mu}|, |\tilde{G}_S^{e\mu}|, |\tilde{G}_P^{e\mu}|\} \in [0, 10^{-9}] \text{ GeV}^{-3}$  and  $\Lambda \in [100, 5000] \text{ GeV}$ . We also show in Fig. 2Parameter space in the  $|G_S^{e\mu}| - \Lambda$  plane. The blue points are these allowed by constraints in Eqs. (2.4equation.2.4) and (2.6equation.2.6).figure.caption.7 the  $|G_S^{e\mu}| - \Lambda$  plane and we identify a small region in which  $|G_{S,P}^{e\mu}| \sim \mathcal{O}(10^{-12} - 10^{-11})$  are particularly favored.

Motivated by these findings, we explore three benchmark points (BMPs) in the next section:

- BMP1:  $|G_S^{e\mu}| = 1.74 \times 10^{-11}$ ,  $|G_P^{e\mu}| = 6.32 \times 10^{-12}$ ,  $|\tilde{G}_S^{e\mu}| = 2.72 \times 10^{-11}$ ,  $|\tilde{G}_P^{e\mu}| = 2.63 \times 10^{-11} \text{ GeV}^{-3}$ ,  $\Lambda = 877 \text{ GeV}$ .
- BMP2:  $|G_S^{e\mu}| = 5.06 \times 10^{-11}$ ,  $|G_P^{e\mu}| = 4.27 \times 10^{-11}$ ,  $|\tilde{G}_S^{e\mu}| = 2.25 \times 10^{-11}$ ,  $|\tilde{G}_P^{e\mu}| = 1.98 \times 10^{-11} \text{ GeV}^{-3}$ ,  $\Lambda = 211 \text{ GeV}$ .
- BMP3:  $|G_S^{e\mu}| = 6.45 \times 10^{-12}$ ,  $|G_P^{e\mu}| = 3.01 \times 10^{-12}$ ,  $|\tilde{G}_S^{e\mu}| = 1.88 \times 10^{-11}$ ,  $|\tilde{G}_P^{e\mu}| = 3.52 \times 10^{-11} \text{ GeV}^{-3}$ ,  $\Lambda = 406 \text{ GeV}$ .

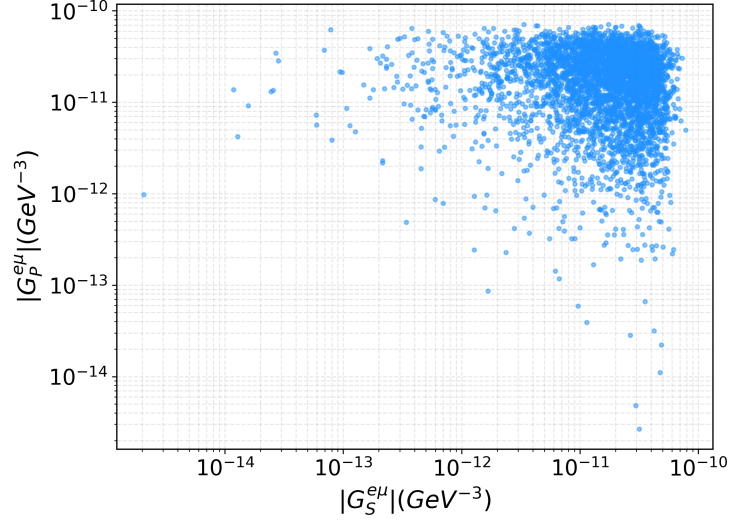


FIG. 1: Parameter space in the  $|G_S^{e\mu}| - |G_P^{e\mu}|$  plane. The blue points are these allowed by constraints in Eqs. (2.4equation.2.4) and (2.6equation.2.6).

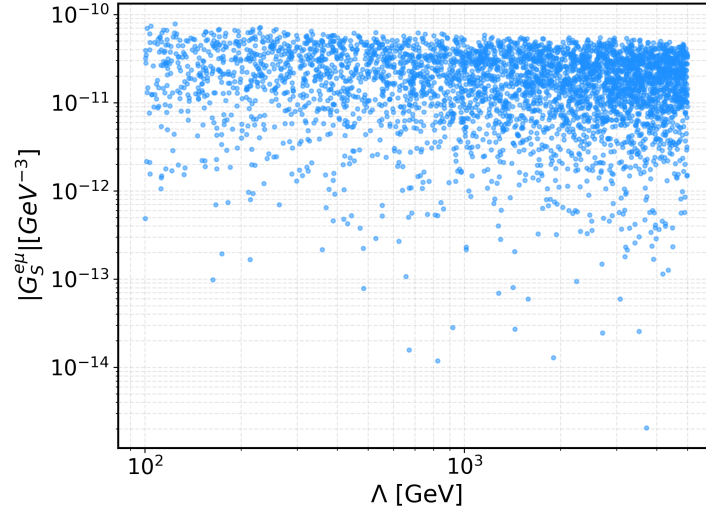


FIG. 2: Parameter space in the  $|G_S^{e\mu}| - \Lambda$  plane. The blue points are these allowed by constraints in Eqs. (2.4equation.2.4) and (2.6equation.2.6).

### III. COLLIDER ANALYSIS

In this section we present a Monte Carlo simulation of the proposed signal, *i.e.*,  $e^-e^+ \rightarrow e^-e^+e\mu$ , as shown in Fig. 3Feynman diagram of the signal  $e^-e^+ \rightarrow e^-e^+e\mu$ . The black circle stands for an effective interaction.figure.caption.9, and its SM background processes.

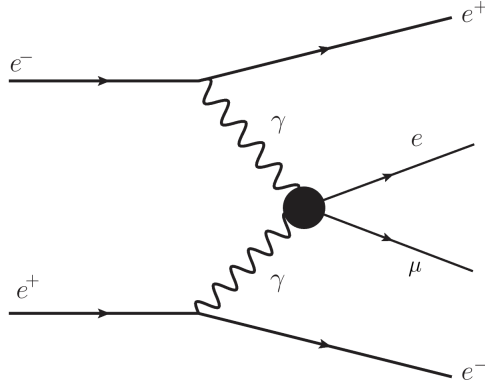


FIG. 3: Feynman diagram of the signal  $e^-e^+ \rightarrow e^-e^+e\mu$ . The black circle stands for an effective interaction.

### A. Signal and background

- *Signal:* We search for a final state  $e^-e^+e\mu$ , where  $e^-$  and  $e^+$  are the scattered electron and positron from the initial state, which are expected to exhibit higher transverse momentum than charged particles ( $e\mu$ ) produced by photon fusion. The study of the complete process is of the utmost importance since the physical information of the  $e^-e^+$  pair of the initial state determines the main features to isolate the signal from the background. In particular, the transverse momentum of the scattered electron is a highlight observable, removing a significant amount of background.

On the other hand, despite suppression of the  $|G_{S,P}^{e\mu}|$  and  $|\tilde{G}_{S,P}^{e\mu}|$  couplings, the signal increases at high center-of-mass energies, as shown in Fig. 4. Production cross section of the signal for the three BMPs (segmented lines) and the dominant SM background (solid lines). The event numbers obtained with an integrated luminosity of  $\mathcal{L}_{\text{int}} = 1 \text{ ab}^{-1}$  are presented on the right axis. Under this finding, both CLIC and ILC would be unbeatable scenarios for the search for the  $\gamma\gamma e\mu$  interaction. Furthermore, both future colliders would be able to produce the signal at the same event level as the background processes, even surpassing them.

- *Background:* Given the very clean environment in  $e^-e^+$  collisions, the dominant SM backgrounds come from  $e^-e^+ \rightarrow e^-e^+e^-e^+$ ,  $e^-e^+ \rightarrow e^-e^+\mu^-\mu^+$ . Other subdominant processes are  $e^-e^+ \rightarrow e^-e^+\pi^-\pi^+$ ,  $e^-e^+ \rightarrow e^-e^+e\mu + \cancel{E}_T$ ,  $e^-e^+ \rightarrow e^-e^+\pi^-\pi^+ + \cancel{E}_T$ , where  $\cancel{E}_T$  stands for missing energy transverse due to neutrinos undetected, which are a product of weak interactions.

Numerical cross sections of the signal and (dominant) background processes are presented in Tables I and II. Production cross sections of the signal  $e^-e^+ \rightarrow e^-e^+e\mu$  for the three BMPs, and cross sections of the dominant SM background, respectively. Meanwhile, Fig. 4 shows the production cross section of the signal for the three BMPs (segmented lines) and the dominant background (solid lines).

nant SM background (solid lines). The event numbers obtained with an integrated luminosity of  $\mathcal{L}_{\text{int}} = 1 \text{ ab}^{-1}$  are presented on the right axis. figure.caption.13 shows an overview of the general behavior of the cross section as a function of the center-of-mass energy. The number of signal and background events produced are also presented.

TABLE I: Production cross sections of the signal  $e^-e^+ \rightarrow e^-e^+e\mu$  for the three BMPs.

BMPs	$\sqrt{s} = 0.5 \text{ TeV}$	$\sqrt{s} = 1 \text{ TeV}$	$\sqrt{s} = 1.5 \text{ TeV}$
BMP1	0.00058 fb	0.018 fb	0.125 fb
BMP2	0.00772 fb	0.2411 fb	1.66 fb
BMP3	0.0000893 fb	0.00279 fb	0.0192 fb

TABLE II: Cross sections of the dominant SM background.

Energy	$\sigma(e^-e^+ \rightarrow e^-e^+e^-e^+)$	$\sigma(e^-e^+ \rightarrow e^-e^+\mu^-\mu^+)$
1.5 TeV	0.64 fb	0.49 fb
1 TeV	1.3 fb	1 fb
0.5 TeV	4.27 fb	3.2 fb

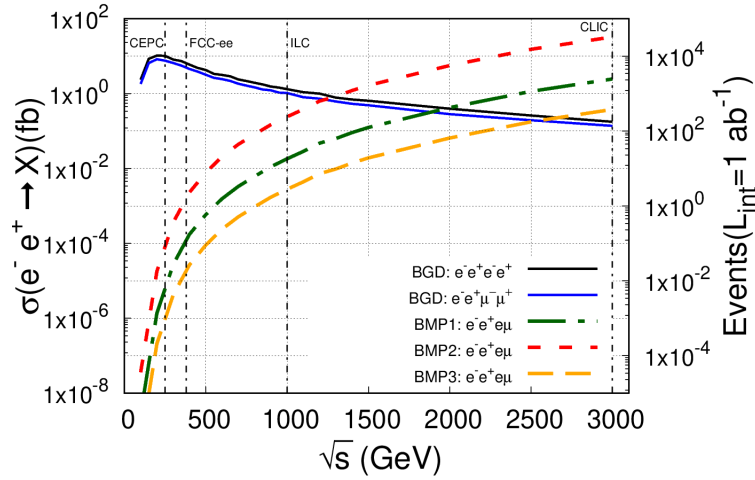


FIG. 4: Production cross section of the signal for the three BMPs (segmented lines) and the dominant SM background (solid lines). The event numbers obtained with an integrated luminosity of  $\mathcal{L}_{\text{int}} = 1 \text{ ab}^{-1}$  are presented on the right axis.

Regarding our computational scheme, we first implement the relevant interactions using LanHEP [27] for MadGraph5 [28]. We then interface the output with Pythia8 [29] and perform detector simulations using Delphes3 [30] with the `delphes_card_ILCgen.tcl` and `delphes_card CLICdet_Stage2.tcl` cards for ILC and CLIC, respectively.

We now turn to calculate the *signal significance* ( $\mathcal{S}$ ), defined as  $\mathcal{S} = N_S / \sqrt{N_S + N_B + (\kappa \cdot N_B)^2}$ , where  $N_S(N_B)$  is the number of signal events (background events) and  $\kappa = 5\%$  is the systematic uncertainty. We compute  $\mathcal{S}$  using **MadAnalysis5** [31] considering the following kinetic cuts:

- $\sqrt{s} = 500$  GeV:
  - $p_T^{e^-} > 100$  GeV,  $p_T^{\mu_1} > 80$  GeV,  $\eta(e^-) < 1.1$  GeV,  $260 < M_{\text{inv}}(e^- \mu_1) < 420$  GeV.
- $\sqrt{s} = 1000$  GeV:
  - $p_T^{e^-} > 200$  GeV,  $p_T^{\mu_1} > 180$  GeV,  $\eta(e^-) < 1.1$  GeV.
- $\sqrt{s} = 1500$  GeV:
  - $p_T^{e^-} > 200$  GeV,  $p_T^{\mu_1} > 180$  GeV,  $\eta(e^-) < 1.1$  GeV,

where  $\mu_1$  represents the muon with the largest transverse momentum.

- In addition, in all cases we require exactly four charged leptons, namely, the  $e^-e^+$  pair coming from the initial state and an  $e\mu$  pair, which has its origin from the central process  $\gamma\gamma e\mu$ .

The corresponding distributions for ILC at  $\sqrt{s} = 1000$  GeV are presented in Fig. 5 Normalized distributions of the signal and dominant background processes: (a) transverse momentum of the scattered electron, (b) transverse momentum of the muon, (c) pseudorapidity of the scattered electron. figure.caption.14. Similar distributions for CLIC were found.

We show in Fig. 6 *Signal significance* as a function of integrated luminosity for CLIC (solid lines) and ILC (dotted lines) for the three BMPs, and center-of-mass energies  $\sqrt{s} = 500, 1000, 1500$  GeV. figure.caption.15 our most outstanding results, *i.e.*, the *signal significance*, which is plotted as a function of the integrated luminosity  $\mathcal{L}_{\text{int}}$  for the three BMPs.

According to the analysis performed, both colliders have the potential to detect the interaction  $\gamma\gamma e\mu$ . In particular, we find that the most promising scenario is BMP2, in which a significance of  $\approx 7\sigma$  ( $\approx 8\sigma$ ) can be achieved once the integrated luminosity search  $\mathcal{L}_{\text{int}} \approx 500 \text{ fb}^{-1}$  ( $\approx 500 \text{ fb}^{-1}$ ) for the future CLIC (ILC), making BMP2 the most favored scenario for experimental searches. Furthermore, BMP2 also offers the possibility of copiously inducing the desired interaction, achieving up to  $40\sigma$  ( $25\sigma$ ) for  $\mathcal{L}_{\text{int}} \approx 2500 \text{ fb}^{-1}$  ( $\mathcal{L}_{\text{int}} \approx 4000 \text{ fb}^{-1}$ ) at CLIC (at ILC). Even if this scenario is considered very optimistic, BMP1 and BMP3 are excellent prospects for proving the existence of the interaction  $\gamma\gamma e\mu$ . The former represents a conservative scenario, but sufficiently encouraging to be able to claim a potential discovery at CLIC at level of  $5\sigma$  if  $\mathcal{L}_{\text{int}} \approx 500 \text{ fb}^{-1}$ . For ILC, we also predict  $\mathcal{S} \approx 5\sigma$ , but a luminosity of  $2500 \text{ fb}^{-1}$  is necessary. As far as BMP3 is concerned, it remains cautious, with a significance around  $5\sigma$  ( $2.5\sigma$ ) for CLIC (ILC) by considering  $\sqrt{s} = 1.5$  TeV ( $\sqrt{s} = 1$  TeV) and an integrated luminosity of  $\mathcal{L}_{\text{inv}} \approx 2500 \text{ fb}^{-1}$  ( $\mathcal{L}_{\text{inv}} \approx 4000 \text{ fb}^{-1}$ ).



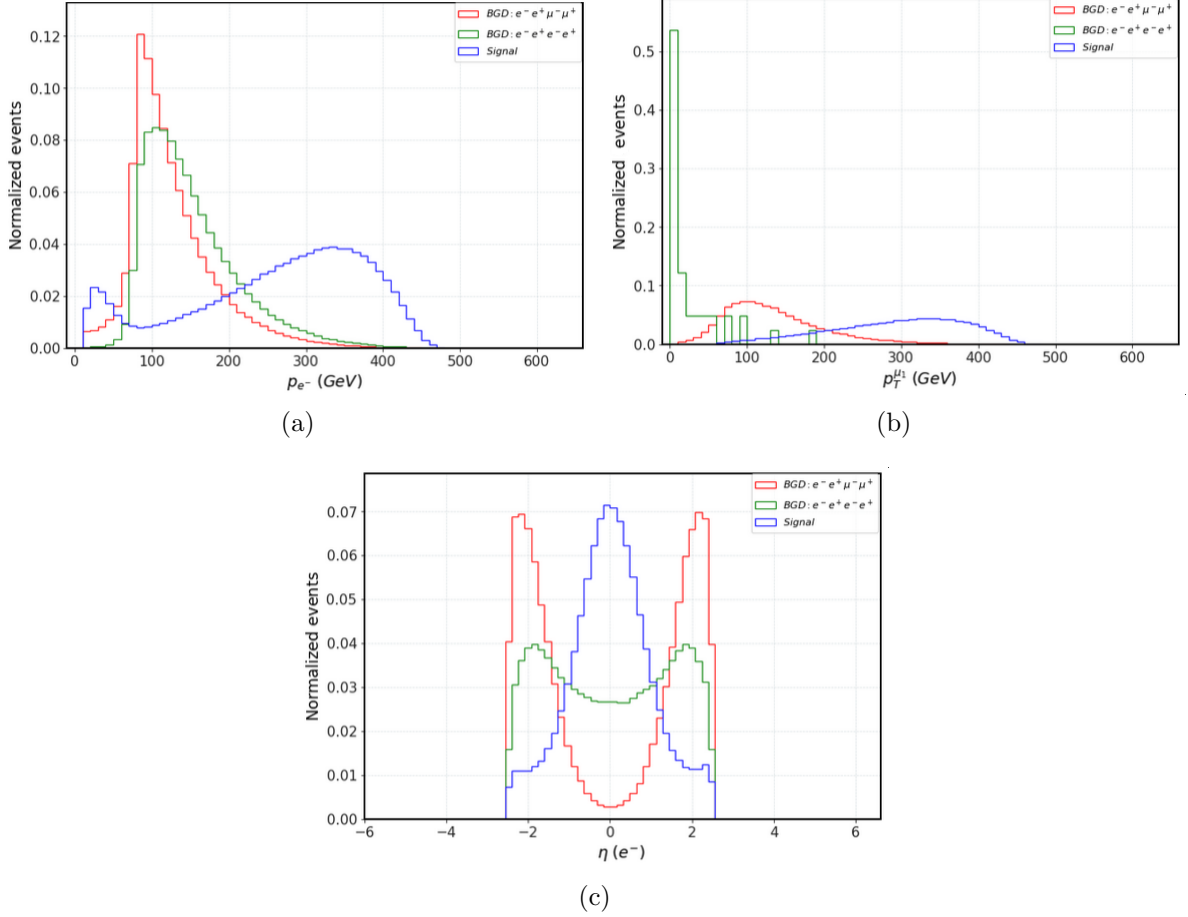


FIG. 5: Normalized distributions of the signal and dominant background processes: (a) transverse momentum of the scattered electron, (b) transverse momentum of the muon, (c) pseudorapidity of the scattered electron.

#### IV. CONCLUSIONS

The search for physics beyond the SM is a key point at collider experiments such as the forthcoming CLIC and ILC. These machines with their high energies, luminosities, and clean experimental environment are particularly well-suited to rigorously analyze the data relevant to the signal proposed in this research. Specifically, we have focused on the lepton flavor-violating process  $e^- e^+ \rightarrow e^- e^+ e \mu$ , where the scattered electron and positron, originating from a peripheral interaction, are accompanied by an  $e\mu$  ( $e = e^-, e^+$ ;  $\mu = \mu^-, \mu^+$ ) pair produced via the effective interaction  $\gamma\gamma e\mu$ . The last reaction is induced by the effective dimension-7 operator, which arises in the low-energy EFT extension of the SM. According to our analysis, the electron in the initial state plays a crucial role in isolating the signal from the background. Under this consideration, our predictions suggest a potential detection of the  $e\mu$  pair produced by electromagnetic interaction, with *signal significances*  $\mathcal{S} \geq 5\sigma$  for specific values of the variables considered in the three BMPs. In particular, we found that the benchmark point 2 (BMP2:  $|G_S^{e\mu}| = 5.06 \times 10^{-11}$ ,  $|G_P^{e\mu}| = 4.27 \times$

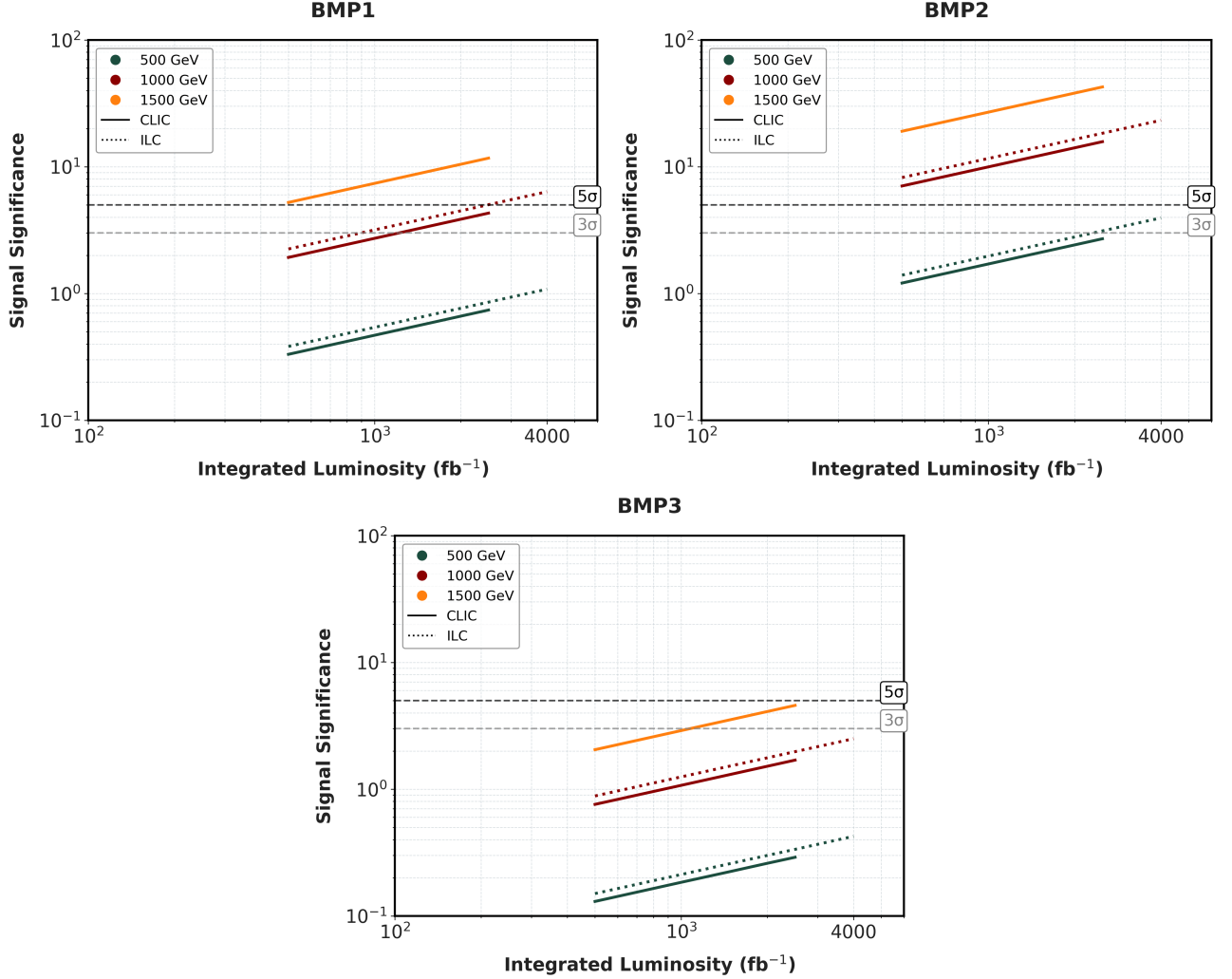


FIG. 6: *Signal significance* as a function of integrated luminosity for CLIC (solid lines) and ILC (dotted lines) for the three BMPs, and center-of-mass energies  $\sqrt{s} = 500, 1000, 1500$  GeV.

$10^{-11}$ ,  $|\tilde{G}_S^{e\mu}| = 2.25 \times 10^{-11}$ ,  $|\tilde{G}_P^{e\mu}| = 1.98 \times 10^{-11} \text{ GeV}^{-3}$ ,  $\Lambda = 211 \text{ GeV}$ .) is the most promising scenario to carry out experimental scrutiny due to the relatively low integrated luminosity and the center-of-mass energy required to achieve  $5\sigma$ , namely,  $\mathcal{L}_{\text{int}} \approx 200 (250) \text{ fb}^{-1}$  and  $\sqrt{s} = 1000 \text{ GeV}$  at ILC (at CLIC). Furthermore, both colliders have the ability to produce the signal copiously increasing either the energy or the integrated luminosity, managing to rediscover for themselves the lepton flavor violation process  $\gamma\gamma e\mu$ .

## ACKNOWLEDGMENTS

Marcela Marín acknowledges support from the UNAM Postdoctoral Program (POSDOC). We are grateful to Michel Hernández Villanueva and Pablo Roig for their invaluable comments. The work of Marco A. Arroyo-Ureña is supported by “Estancias Posdoctorales por México (SE-

CIHTI)” and “Sistema Nacional de Investigadores e Investigadoras”. M. G. Villanueva-Utrilla and Humberto Salazar thank to Vicerrectoría de Investigación y Estudios de Posgrado through “Centro Interdisciplinario de Investigación y Enseñanza de la Ciencia” (CIEC).

- 
- [1] Y. Fukuda et al. (Super-Kamiokande), *Phys. Rev. Lett.* **81**, 1562 (1998), [arXiv:hep-ex/9807003](#).
  - [2] Q. R. Ahmad et al. (SNO), *Phys. Rev. Lett.* **87**, 071301 (2001), [arXiv:nucl-ex/0106015](#).
  - [3] Q. R. Ahmad et al. (SNO), *Phys. Rev. Lett.* **89**, 011301 (2002), [arXiv:nucl-ex/0204008](#).
  - [4] S. T. Petcov, *Sov. J. Nucl. Phys.* **25**, 340 (1977), [Erratum: *Sov.J.Nucl.Phys.* 25, 698 (1977), Erratum: *Yad.Fiz.* 25, 1336 (1977)].
  - [5] E. Diociaiuti (Mu2e), *PoS WIFAI2023*, 017 (2024).
  - [6] A. Blondel et al., (2013), [arXiv:1301.6113 \[physics.ins-det\]](#).
  - [7] W. Altmannshofer et al. (Belle-II), *PTEP* **2019**, 123C01 (2019), [Erratum: *PTEP* 2020, 029201 (2020)], [arXiv:1808.10567 \[hep-ex\]](#).
  - [8] E. Adli et al., (2025), [arXiv:2503.24168 \[physics.acc-ph\]](#).
  - [9] A. Aryshev et al. (ILC International Development Team), (2022), [arXiv:2203.07622 \[physics.acc-ph\]](#).
  - [10] V. M. Budnev, I. F. Ginzburg, G. V. Meledin, and V. G. Serbo, *Phys. Rept.* **15**, 181 (1975).
  - [11] C. F. von Weizsacker, *Z. Phys.* **88**, 612 (1934).
  - [12] E. J. Williams, *Phys. Rev.* **45**, 729 (1934).
  - [13] D. d’Enterria and G. G. da Silveira, *Phys. Rev. Lett.* **111**, 080405 (2013), [Erratum: *Phys.Rev.Lett.* 116, 129901 (2016)], [arXiv:1305.7142 \[hep-ph\]](#).
  - [14] G. Aad et al. (ATLAS), *Phys. Rev. Lett.* **123**, 052001 (2019), [arXiv:1904.03536 \[hep-ex\]](#).
  - [15] A. M. Sirunyan et al. (CMS), *Phys. Lett. B* **797**, 134826 (2019), [arXiv:1810.04602 \[hep-ex\]](#).
  - [16] S. Chatrchyan et al. (CMS), *JHEP* **01**, 052 (2012), [arXiv:1111.5536 \[hep-ex\]](#).
  - [17] G. Aad et al. (ATLAS), *Phys. Lett. B* **749**, 242 (2015), [arXiv:1506.07098 \[hep-ex\]](#).
  - [18] W. Abdallah et al. (CEPC Study Group), *Radiat. Detect. Technol. Methods* **8**, 1 (2024), [Erratum: *Radiat.Detect.Technol.Methods* 9, 184–192 (2025)], [arXiv:2312.14363 \[physics.acc-ph\]](#).
  - [19] A. Abada et al. (FCC), *Eur. Phys. J. ST* **228**, 261 (2019).
  - [20] F. Fortuna, X. Marcano, M. Marín, and P. Roig, *Phys. Rev. D* **108**, 015008 (2023), [arXiv:2305.04974 \[hep-ph\]](#).
  - [21] A. M. Baldini et al. (MEG), *Eur. Phys. J. C* **76**, 434 (2016), [arXiv:1605.05081 \[hep-ex\]](#).
  - [22] B. Aubert et al. (BaBar), *Phys. Rev. Lett.* **104**, 021802 (2010), [arXiv:0908.2381 \[hep-ex\]](#).
  - [23] A. Abdesselam et al. (Belle), *JHEP* **10**, 19 (2021), [arXiv:2103.12994 \[hep-ex\]](#).

- [24] J. D. Bowman, T. P. Cheng, L.-F. Li, and H. S. Matis, *Phys. Rev. Lett.* **41**, 442 (1978).
- [25] S. Davidson, Y. Kuno, Y. Uesaka, and M. Yamanaka, *Phys. Rev. D* **102**, 115043 (2020), [arXiv:2007.09612 \[hep-ph\]](#).
- [26] F. Fortuna, A. Ibarra, X. Marcano, M. Marín, and P. Roig, *Phys. Rev. D* **107**, 015027 (2023), [arXiv:2210.05703 \[hep-ph\]](#).
- [27] A. Semenov, *Comput. Phys. Commun.* **201**, 167 (2016), [arXiv:1412.5016 \[physics.comp-ph\]](#).
- [28] J. Alwall, M. Herquet, F. Maltoni, O. Mattelaer, and T. Stelzer, *Journal of High Energy Physics* **2011** (2011), [10.1007/jhep06\(2011\)128](#).
- [29] T. Sjöstrand, S. Ask, J. R. Christiansen, R. Corke, N. Desai, P. Ilten, S. Mrenna, S. Prestel, C. O. Rasmussen, and P. Z. Skands, *Comput. Phys. Commun.* **191**, 159 (2015), [arXiv:1410.3012 \[hep-ph\]](#).
- [30] J. de Favereau, C. Delaere, P. Demin, A. Giammanco, V. Lemaître, A. Mertens, and M. Selvaggi (DELPHES 3), *JHEP* **02**, 057 (2014), [arXiv:1307.6346 \[hep-ex\]](#).
- [31] E. Conte, B. Fuks, and G. Serret, *Comput. Phys. Commun.* **184**, 222 (2013), [arXiv:1206.1599 \[hep-ph\]](#).